Iranian Journal of Science and Technology, Transactions of Civil Engineering
https://doi.org/10.1007/s40996-023-01066-1

RESEARCH PAPER

The Influence of Ground and Unground Rice Husk Ash on The Physico-mechanical and Microstructural Properties of Cement Mortars

Abbas Tiambo Datchossa[1] · Valéry K. Doko[1] · Nihat Kabay[2] · Emmanuel E. T. Olodo[1] · Tarik Omur[2]

Received: 21 October 2022 / Accepted: 6 February 2023

Abstract

Superseding a portion of cement with agricultural wastes like rice husk ash (RHA) is an excellent solution to alleviate the ecological issues and resource depletion induced by cement production. In this paper, cement-based mortars were produced where Portland cement was replaced with ground or unground RHA (GRHA or URHA) from 0 to 12.5 wt% with an increment of 2.5% to investigate their effect on the fresh, physical, mechanical, and microstructural properties of mortars. GRHA inclusion up to 10% was advantageous due to the ameliorated physico-mechanical properties compared to other mixtures. In contrast, the introduction of URHA negatively affected the physical properties of mortars; however, the compressive strength values of URHA-containing mixtures were comparable to those of reference and GRHA mixes up to 7.5% replacement ratio. The macro-pores of mortars reduced with the incorporation of 10% GRHA or URHA, whereas the total porosity value increased with 10% URHA inclusion. The microstructural analysis suggested that the utilization of both GRHA and URHA decreased the portlandite content due to pozzolanic reactions. Hence, a relatively low amount of URHA compared to GRHA can also be efficiently used to produce mortar mixes without additional energy consumption and expense resulting from grinding.

Keywords Mechanical properties · Physical properties · Microstructural · Rice husk ash · Grinding

1 Introduction

The environmental problems brought about by global warming and the depletion of raw materials used in the construction sector have revealed the attempt to utilize eco-friendly materials at higher rates globally (Abdulmatin et al. 2022; Jongpradist et al. 2018; Mounika et al. 2022; Snehal et al. 2022; Tuoi Nguyen et al. 2022). Agricultural waste is one of these eco-friendly materials, which is an alternative to use as a binder in concrete or mortar production. Due to the low charge of agricultural wastes, their economical values are significantly lower than the expense of collecting, transporting, and treating them for beneficial use (Gil-Carrera et al. 2019). Each year, approximately one billion tons of these solid wastes are generated, and this figure is rising (Moayedi et al. 2019; Mymrin et al. 2018).

The exterior of rice grain, also known as rice husk, is a widely known agricultural waste or by-product in many regions around the world. It is a by-product of rice milling factories, and the combustion of rice husk generates significant amount of rice husk ash (RHA) (Jamil et al. 2013a). RHA has voiced ecological issues since it can cause health problems for local residents nearby (Hadipramana et al. 2016). Rice production is expected to increase in the future due to the growing population and increased nutrition demand (Mukharjee & Patra 2022). The rice mills produce approximately 20% rice husk for each ton of paddy, which is utilized as an energy source in the boiler. After processing, around 25% of the rice husk transforms into RHA (Hadipramana et al. 2016). In addition, the cellulose–lignin structure of rice husk extinguishes during combustion, leaving only a highly porous structure. Hence, RHA contains a substantial amount of silica, thereby it is considered as a pozzolanic material in the manufacturing of cementitious matrix (Jamil et al. 2013).

✉ Tarik Omur
tomur@yildiz.edu.tr

[1] Laboratory of Energetics and Applied Mechanics (LEMA), University of Abomey-Calavi, Abomey-Calavi, Benin

[2] Construction Materials Division, Department of Civil Engineering, Yildiz Technical University, 34220 Istanbul, Turkey

Published online: 25 February 2023

RHA has been mainly utilized as a supplementary cementitious material in the production of concrete due to the combination of its pozzolanic and filler properties (Cordeiro et al. 2009; Nair et al. 2008; Zain et al. 2011). Besides, it has been used as a silica source which facilitates the geopolymeric reactions in the alkali activation process (Bouzón et al. 2014; Fernando et al. 2021). The extraction of silica from RHA is an economical process, and this property alleviates its utilization in the preparation of alkaline solution and also in some other industries such as cosmetics, and food (Sarangi et al. 2009). In addition, RHA has been used in soil stabilization along with lime because of the economic advantages and its compatible chemical composition (Moayedi et al. 2019).

Several authors have already shown the potential use of RHA on the aforementioned areas. Malhotra and Mehta (1996) investigated how the pozzolanic activity of RHA results from its pyroprocessing and confirmed that combustion of rice husk under planned burning circumstances could yield RHA that was abundant in amorphous silica. It was also found that the pozzolanic properties of RHA can be improved when the time and temperature of burning process were adjusted (Ferraro et al. 2010). Costa and Paranhos (2018) examined two different rice sources in order to obtain desired amorphous silica content of RHA by using various burning conditions, and found that the amorphous silica content can be adjusted with the appropriate rice type and combustion parameters. It was revealed that the optimum burning parameters for rice husks were determined as 2 h at 700 °C. On the other hand, uncontrolled open-air combustion of rice husk results in a high amount of carbon in RHA, which can have a negative impact on the characteristics of cement-based materials and create a highly crystalline microstructure (Siddika et al. 2021). Depending on the burning time and temperature, amorphous characteristics of RHA can be varied and thereby the mechanical, physical, and durability properties of cementitious mixes incorporating RHA may be affected (Liu et al. 2016).

Another significant parameter on the reactivity of RHA is its fineness. The increase in the fineness increases the reactivity of RHA as a pozzolanic material in cementitious matrix (Antiohos et al. 2014). However, it was also reported that the grinding of RHA could enhance the pozzolanic property up to a certain particle size (Zerbino et al. 2011). Therefore, excessive grinding of amorphous RHA should be evaded because its pozzolanic property is primarily derived from the interior surface area of its particles (Malhotra and Mehta 1996). Abu Bakar et al. (2011) studied the effect of the grinding time of RHA on the physical and mechanical properties of concrete samples and found that the longer grinding times (> 90 min) induced significantly higher fineness and specific surface area for RHA particles which caused higher water demand and consequently lower strength activity index and compressive strength values. Several authors have investigated the mechanical and physical characteristics of cementitious composites containing RHA; however, there is a limited study which emphasize the effect of unground RHA (URHA) (i.e., direct utilization) and ground RHA (GRHA) on the properties of cement mortar. Hence, this study aims to comparatively investigate the effect of URHA or GRHA on the mechanical and physical characteristics of cement mortars. In addition, the microstructural properties such as thermogravimetric analysis (TGA), mercury intrusion porosimetry (MIP), and X-ray diffractometer (XRD) were also investigated to deduce the effects of RHA on cement-based mortars.

2 Experimental Scheme

2.1 Raw Materials

CEM I 42.5R grade Portland cement (PC) and two types of RHA (URHA, GRHA) were used as the binding materials in the preparation of mortar samples. PC was procured from a local market located in Istanbul, Turkey. RHA is obtained by calcining rice husks at a temperature of 600 °C for 2 h, and raw rice husks were collected from a local paddy mill located in Benin. The physical appearances of raw rice husk and RHAs are depicted in Fig. 1. The scanning electron microscopy (SEM) images of raw RHAs are depicted in Fig. 2. It was observed that both GRHA and URHA have

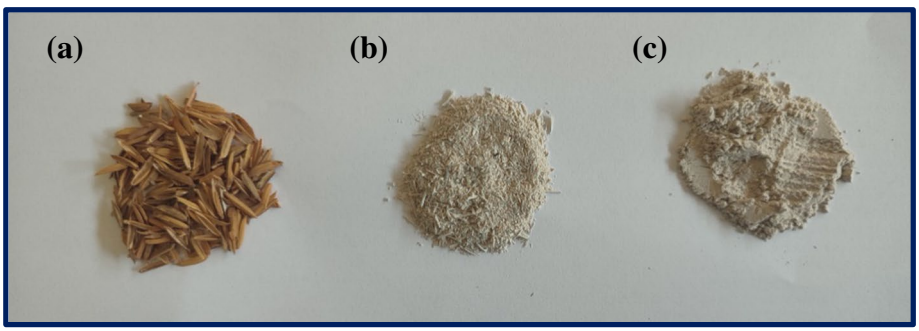

Fig. 1 Appearances of: **a** raw rice husk, **b** URHA, and **c** GRHA

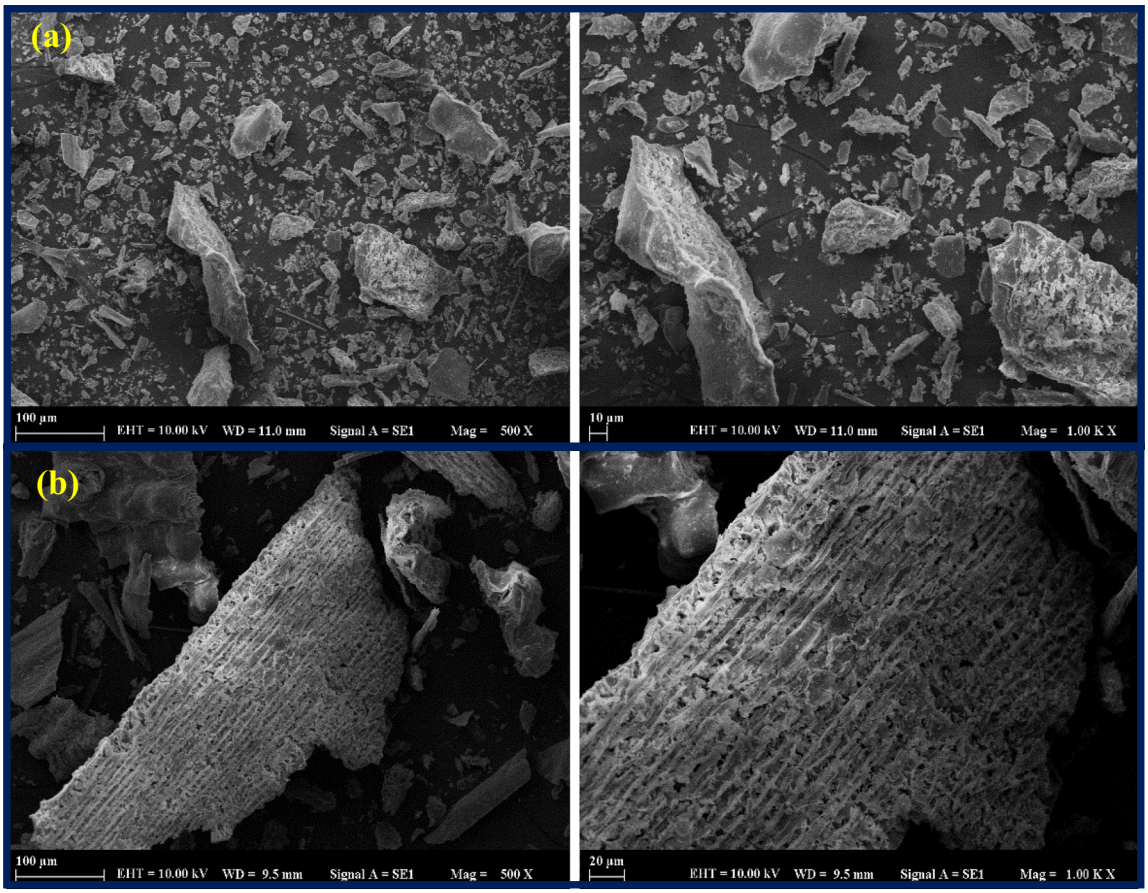

Fig. 2 SEM appearances of raw RHAs: **a** GRHA and **b** URHA

irregularly shaped particles with varying range of sizes. GRHA exhibited more compact and less porous structure with finer particles compared to URHA, which has a highly porous cellular structure. The calcination process of raw rice husks consisted of two different phases. In the first hour, the temperature was increased up to 600 °C in the oven. Subsequently, the oven temperature was maintained at 600 °C for 1 h. URHA was obtained after the calcination process and directly utilized as in ash form without any grinding process, whereas GRHA was ground using a laboratory-type mill grinder. The oxide components and the particle size distribution (PSD) curves of binders and sand are illustrated in Table 1 and Fig. 3, respectively. PC was mainly consisted of CaO and SiO_2, while the major chemical oxide of RHA was SiO_2 with a total of 86.46%. Locally sourced natural siliceous sand was employed as fine aggregate to produce mortar specimens.

Table 1 The chemical components of binding materials

Oxide composition (%)	PC	RHA
CaO	63.14	2.64
SiO_2	20.23	86.46
Al_2O_3	5.14	1.27
Fe_2O_3	3.87	0.59
MgO	1.25	0.47
Na_2O	0.26	0.06
K_2O	0.83	1.37
SO_3	2.89	0.25
Loss on ignition	1.55	6.35
Others	0.84	0.54

2.2 Preparation of Mortar Samples and Testing Procedures

The mix design parameters and mixture codes of mortar samples are tabulated in Table 2. In order to observe the effect of grinding on the mechanical and physical characteristics of cement mortar specimens, URHA or GRHA replaced PC at a ratio of 2.5%, 5%, 7.5%, and up to 12.5% by weight of cementitious materials. The alphabetical part of specimen IDs represents the RHA type used, while the numerical part demonstrates the replacement ratio of RHA. 'REF' indicates the plain mortar mixture without any RHA. The sand to binder (s/b) and water to binder (w/b) ratios

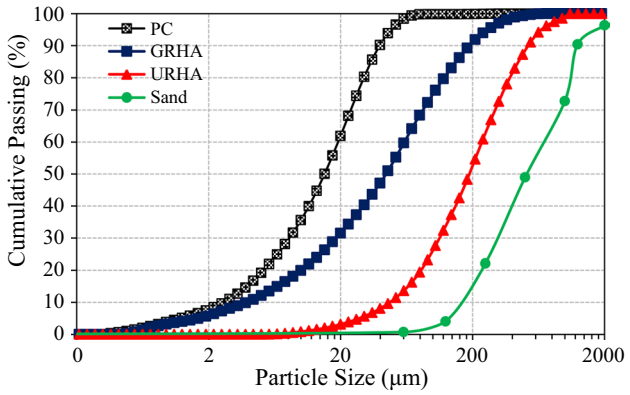

Fig. 3 Particle size distribution of raw materials

Table 2 Mix design parameters of mortar specimens

Mortar IDs	PC (%)	URHA (%)	GRHA (%)	s/b (wt.)	w/b (wt.)
REF	100	–	–	3	0.6
URHA-2.5	97.5	2.5	–		
URHA-5	95	5	–		
URHA-7.5	92.5	7.5	–		
URHA-10	90	10	–		
URHA-12.5	87.5	12.5	–		
GRHA-2.5	97.5	–	2.5		
GRHA-5	95	–	5		
GRHA-7.5	92.5	–	7.5		
GRHA-10	90	–	10		
GRHA-12.5	87.5	–	12.5		

were maintained as 3.0 and 0.6 for each mix, respectively. The mortar mixes were manufactured in accordance with NF EN 196 standard. Initially, dry mixing was conducted in a mixer bowl by introducing binding materials and natural sand and then water was added into the mixture. The mixing process was continued for about 3 min to attain homogenous moldable mixes. The fresh mortar mixes were poured into $50\times50\times50$ mm^3 cubic molds, and after 24 h of casting, the molds were removed and the specimens cured in water until the designated testing age to determine the physical and mechanical properties.

SEM analysis was conducted to investigate the morphology of the raw RHA particles by using Zeiss EVO® LS 10 SEM instrument (Carl Zeiss Microscopy GmbH, Germany).

The flowability and density of fresh mortar mixes were determined according to NF EN 1015-3 and NF EN 1015-6, respectively. To determine the flowability, the fresh mortars were poured into the truncated cone mold as two layers, and each layer was compacted with 10 short strokes of the tamper to assure consistent filling of the mold. Subsequently, the conic mold was vertically removed, and the flow table was dropped 15 times. The spreading diameters were measured along the mortar diameter in two directions using a caliper. The test results are presented as the increment in the spreading diameter of fresh mortar mix according to the base diameter of the cone mold using Eq. (1).

$$E(\%) = \frac{d_r - d_i}{d_i} \times 100 \tag{1}$$

where d_r represents the spreading diameter of fresh mortar mix and d_i demonstrates the base diameter of the truncated cone mold (10 cm).

To determine the fresh density, an empty container having a volume of 'V' was weighted and its mass was recorded as m_1. The fresh mortar mix was cast into the container and vibrated until no further settling can be observed. The weight of the fresh mortar mix was then measured and recorded as m_2. The fresh density of mortars can be determined as per Eq. (2).

$$\rho = \frac{m_2 - m_1}{V} \tag{2}$$

The physical characteristics of hardened mortars such as density, the absorption coefficient, and the apparent porosity were determined using ASTM C948 standard. The hardened mortar samples were saturated in water until a constant mass was obtained. The saturated-surface dried (SSD) mortar samples were weighted in water (m_1) and air (m_2), and consequently, their volumes were determined. Hereafter, the samples were dried (m_3) in an oven at 105 °C for about 24 h. The hardened physical properties of mortars were determined using Eqs. (3–5).

$$\rho_{\text{sec}} = \frac{m_3}{m_2 - m_1} \tag{3}$$

$$A_b = \frac{m_2 - m_3}{m_3} \times 100. \tag{4}$$

$$p = \frac{m_2 - m_3}{m_2 - m_1} \times 100. \tag{5}$$

In these equations, ρ_{sec}, A_b, and p show the hardened density, absorption coefficient, and apparent porosity of mortar specimens, respectively. In addition, compressive strength of mortars was tested at 7 and 28 days of curing age using three plicate specimens with dimensions of $50\times50\times50$ mm^3.

Star TG/DTA 6300 equipment (Seiko, Japan) was employed to deduce the heat flow and mass loss with the increasing temperature. The exact limits of the temperature ranges were determined by the differential thermogravimetry (DTG). The test was conducted in an inert nitrogen ambient, and the specimens were heated from 25 to 1000 °C at a rate of 10 °C per minute. The amount of $Ca(OH)_2$ within the

samples was calculated according to the method proposed by (Chithra et al. 2016; Snehal et al. 2022; Singh et al. 2015; Snehal et al. 2020a, b) using the Eq. (6).

$$Ca(OH)_2(\%) = \frac{Mw_{CH}}{Mw_w} \times ML(CH) \quad (6)$$

where Mw_{CH} and Mw_w represent the molecular mass of $Ca(OH)_2$ and water, respectively. ML(CH) is the percentage mass loss due to the $Ca(OH)_2$ dehydration, which corresponds to peaks at around 400 °C in TG plots.

The PANalytical X'Pert PRO diffractometer was employed to define the mineralogical structures. The diffraction peaks were determined with an interval of 0.017° (step size) and a scanning interval of 5–90° (2θ).

The pore structure of the mortar specimens was assessed with the Mercury intrusion porosimetry (MIP) method operating a Pore Master (Quantachrome Instruments) porosimeter from 0 to 58,000 psi. The contact angle between mercury and pore surfaces is assumed as 140° during the intrusion.

3 Results and Discussion

3.1 Fresh Properties

3.1.1 Flowability

Figure 4 plots the effect of URHA or GRHA replacement on the flowability of mortar mixtures. The descending trend was observed on the flow curves for both GRHA and URHA replacement in which the increase in the RHA ratio consistently reduced the flowability of mixes. While the flow percentages of the mortars including GRHA decreased almost linearly, a logarithmic trend was observed in the mixtures containing URHA, with a significant decrease in the 5% replacement ratio. The reduced flowability with the higher RHA ratios can be attributed to the hydrophilic nature of RHA particles compared to PC particles (Antiohos et al. 2014), which reduces contact angle between water and particle surface and increases the water demand of mortar mixes. It was previously reported that the grinding process on RHA led to forming of finely shaped and compact particle structures as illustrated in Fig. 2. (Abu Bakar et al. 2011). Therefore, the inclusion of URHA led to higher reduction on flow values of mortars compared to GRHA mixes which is possibly due to their irregular particle shape and higher porous cellular structure of URHA particles which create a greater water demand (see Fig. 2).

3.1.2 Fresh Density

Figure 5 shows the fresh density evolution of RHA substituted mortar mixes. The fresh densities of mortar mixes containing GRHA varied between 2076 and 2168 kg/m^3, while the fresh densities of mixtures with URHA ranged between 1909 and 2136 kg/m^3. It was also determined as 2169 kg/m^3 for control mixture. The replacement of GRHA with cement led to reduction of the fresh densities of mortars up to 4.3%. On the other hand, the effect of URHA was more pronounced and the incorporation of URHA consistently decreased the fresh densities up to 12.0%. It can be observed that RHA particles contain intrinsic macro- and mesopores inside (Fig. 2), which can be diminished with higher fineness. After grinding process, the closed macro- and mesopores of the RHA particles were reduced and more compact structure were obtained. This also led to an increase in the specific gravity of RHA particles (Abu Bakar et al. 2011). The drop of fresh density with higher RHA replacement ratio can be attributed to this interior porosity and the higher amount of pores in the URHA particles resulted

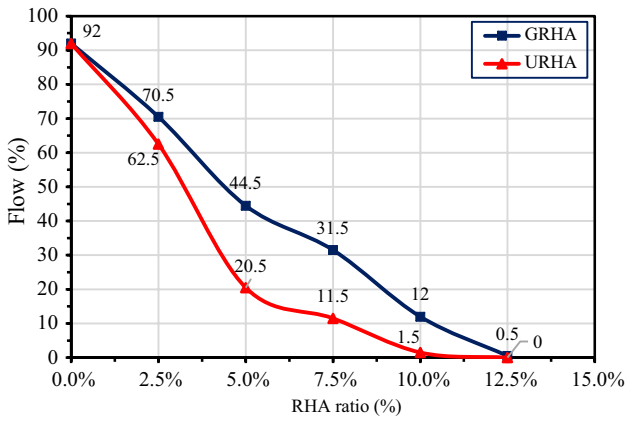

Fig. 4 The effect of URHA and GRHA replacement on the flow values of mortars

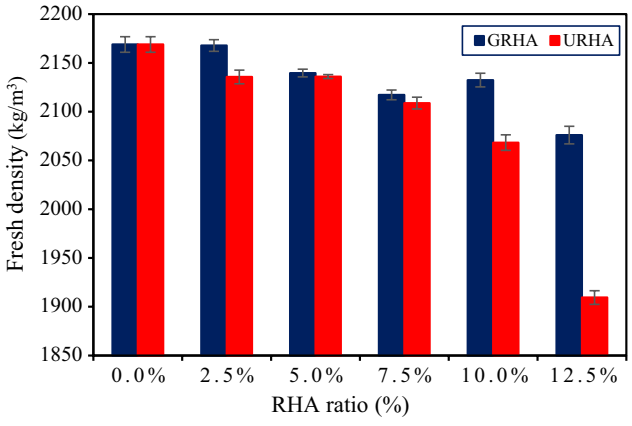

Fig. 5 The fresh density of mortars with URHA or GRHA replacement

in higher fresh density reduction on mortars compared to GRHA mixtures.

3.2 Hardened Properties

3.2.1 Hardened Density of Mortars

The change in the hardened density of mortars at 7 days is depicted in Fig. 6a. GRHA substituted mixes exhibited higher density when compared to the reference mixture, whereas the densities of mortars with URHA were found to be generally lower than the reference. This is possibly owing to the more pronounced pozzolanic effect of GRHA at early reaction ages. It has been reported that RHA shows better pozzolanic activity compared to conventional supplementary cementitious materials such as blast furnace slag and fly ash due to its amorphous structure and finer particles, which facilitate the formation of strength giving reaction products such as calcium silicate hydrate (C–S–H) gels at early reaction ages (Feng et al. 2004). Considering the fact that the finer RHA particles result in higher pozzolanic activity and that they can contribute to the refinement of matrix pore structure (Antiohos et al. 2014), they might have revealed higher density values in mortars containing GRHA compared to the reference and URHA mixes. On the other hand, lower densities of URHA-incorporated mortars compared to the REF mortar can be credited to the lower pozzolanic activity and higher intrinsic particle porosity. Furthermore, the hardened density of mortars significantly dropped beyond 10% of URHA replacement due to the dominance effect of lower specific gravity of URHA due to the porous structure as compared to PC.

Figure 6b shows the evolution of hardened density values of mortars at 28 days. It was observed that the hardened densities of mortars at 28 days were overall greater than that of 7 days. While an increase was observed in the density values of the mortars up to 10% GRHA replacement, the density of mortars decreased when GRHA replacement was 12.5%. Similar findings were previously observed by Isberto et al. (2019). This increase could be explained by two main properties of RHA in the mixture: (i) filler effect and (ii) pozzolanic feature. The former allows to fill the intergranular voids by fine RHA particles (i.e., GRHA), the latter allows the transformation of portlandite ($Ca(OH_2)$) into C–S–H gels which is comparatively a denser reaction product than portlandite. On the other hand, the sudden decrease in the hardened density after 10% of GRHA replacement could result from the lower flowability of mortars, which can lead to macro-pores in the samples. The mortar densities of URHA mixtures generally remain low as compared to GRHA mortars for their corresponding replacement ratios and the increase in the URHA ratio reduced the density of mortars. This is possibly resulting from the lower filler properties and more porous structure of URHA particles compared to GRHA (Mounika et al. 2022; Sanou et al. 2019; Zaid et al. 2021).

3.2.2 Porosity and Water Absorption

Figures 7 and 8 illustrate the variation of mortar porosity and water absorption values at 7 and 28 days of curing age, respectively. The porosity values ranged between 13.56–18.90% and 15.00–26.85% at 28 days for GRHA and URHA incorporated mixtures, respectively. The porosity

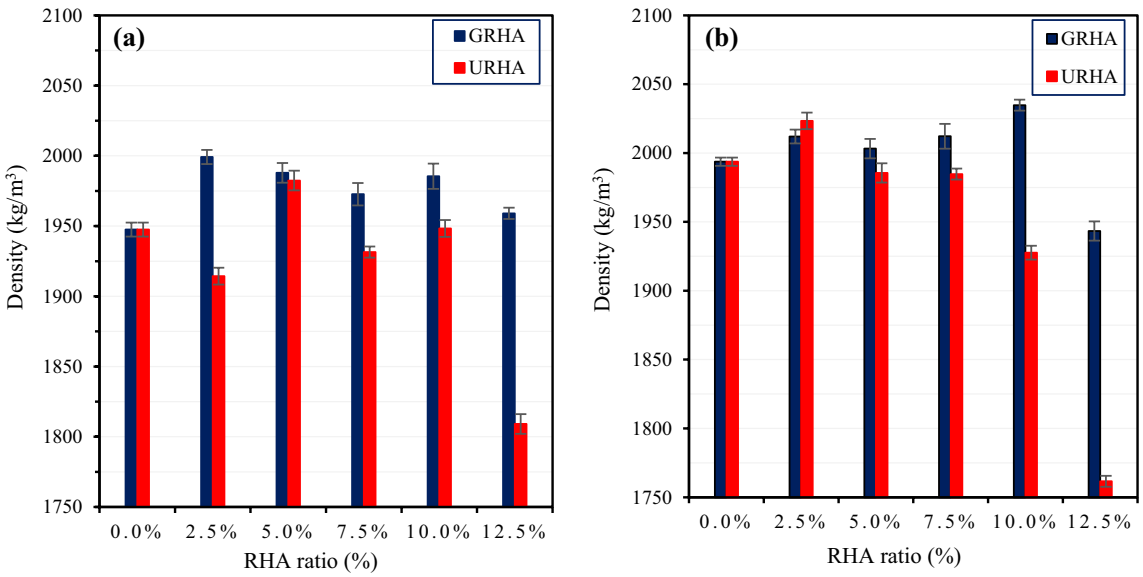

Fig. 6 The variation of the hardened density values of mortars at: **a** 7 days, **b** 28 days

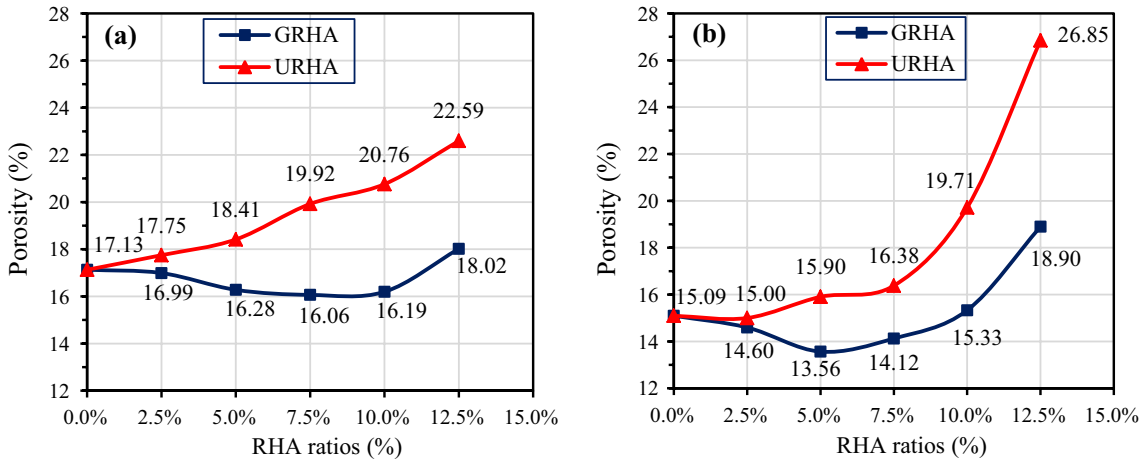

Fig. 7 Evolution of porosity on hardened mortar samples at: **a** 7 days, and **b** 28 days

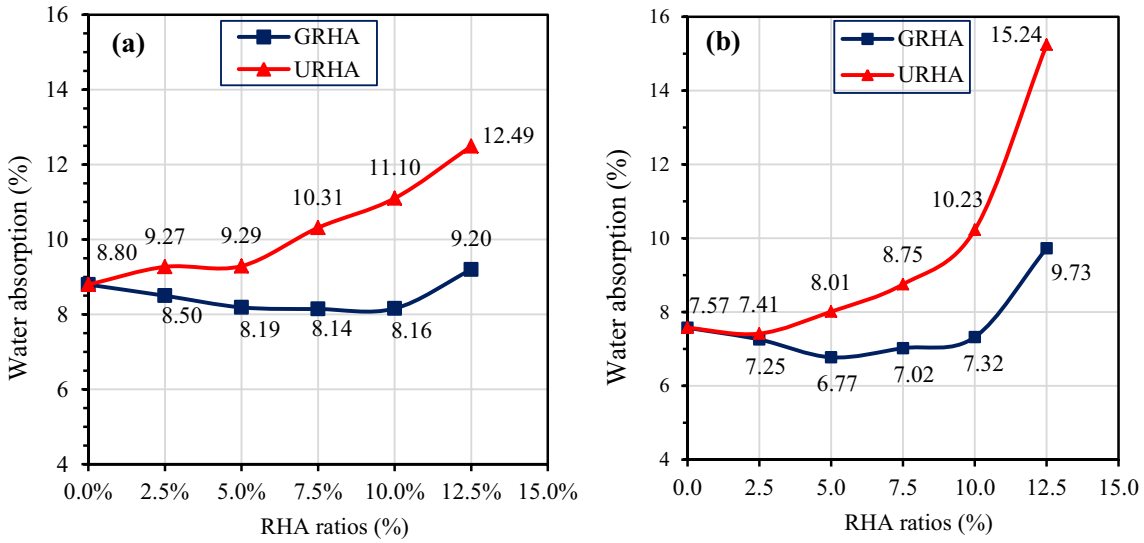

Fig. 8 The water absorption of mortar specimens at: **a** 7 days, and **b** 28 days

values of the mortar samples incorporating RHA up to 10% reduced from 7 to 28 days due to the progress of hydration reactions. On the other hand, the porosity of 12.5% GRHA and URHA-containing mixes increased at 28 days compared to their values at 7 days. The porosity of mortars consistently increased with an increase in the replacement ratio of URHA at both 7 and 28 days, whereas the GRHA yields lower or comparable porosity up to 10% replacement ratio at 7 and 28 days, compared to the REF mixture. As such, the incorporation of GRHA reduced the porosity up to 6.2% (7 days) and 10.1% (28 days), while the porosity increased up to 31.8% and 77.9% with the inclusion of URHA at 7 and 28 days, respectively. This might be possibly due to the higher intrinsic porosity of URHA compared to GRHA (Fig. 2). The porosity values are found to be in well agreement with the hardened density results (Fig. 9a) in which the higher density resulted in a decrease in porosity of mortars and vice versa. Table 3 shows the established regression equations and R^2 values between physical and mechanical properties of mortar mixes. The relationship between porosity and density was statistically insignificant at 7 days with lower R^2 values; however, 28th days test results indicated that porosity and density values exhibited statistically significant relationship with higher R^2 values.

Similar to porosity values, water absorption of mortars showed a reduction with increase in curing age, except for mortars containing 12.5% RHA. The water absorption of mixes was exponentially increased with the higher URHA substitution at 7 and 28 days, while the higher replacement ratios of GRHA induced lower water absorption values

up to 10% at 7 and 28 days, compared to the REF mixture. The highest water absorption values were observed at 12.5% replacement ratio of PC with GRHA or URHA and found as 9.73% and 15.24%, respectively. The relationship between porosity and water absorption values of mortars is illustrated in Fig. 9b showing a linear correlation with the R^2 values of greater than 0.97, irrespective of RHA type and curing age.

3.2.3 Compressive Strength

The compressive strength development of mortars is depicted in Fig. 10. It can be noticed that the compressive strength of mortars containing GRHA or URHA increased with increasing curing time and the increment was notable at higher RHA inclusion. The compressive strength of GRHA-incorporated mortars increased in the range between 2 and

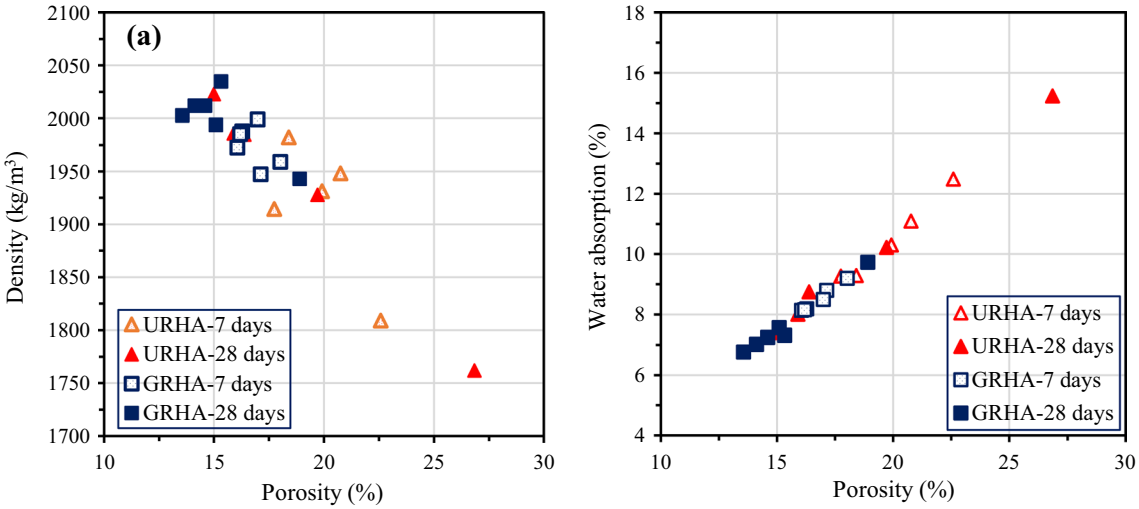

Fig. 9 The correlation between porosity and **a** density, **b** water absorption

Table 3 The statistical relationship between tested parameters

RHA type/Test age	Porosity-density		Porosity-water absorption		Density-compressive strength	
URHA-7 days	$y=-20.1x+2312$	$R^2=0.48$	$y=0.67x-2.8$	$R^2=0.98$	$y=0.11x-193$	$R^2=0.61$
URHA-28 days	$y=-20.6x+2321$	$R^2=0.99$	$y=0.65x-2.2$	$R^2=0.99$	$y=0.08x-125$	$R^2=0.95$
GRHA-7 days	$y=-12.5x+2185$	$R^2=0.24$	$y=0.56x-0.9$	$R^2=0.97$	$y=0.17x-300$	$R^2=0.27$
GRHA-28 days	$y=-12.9x+2197$	$R^2=0.62$	$y=0.56x-0.9$	$R^2=0.98$	$y=0.16x-295$	$R^2=0.95$

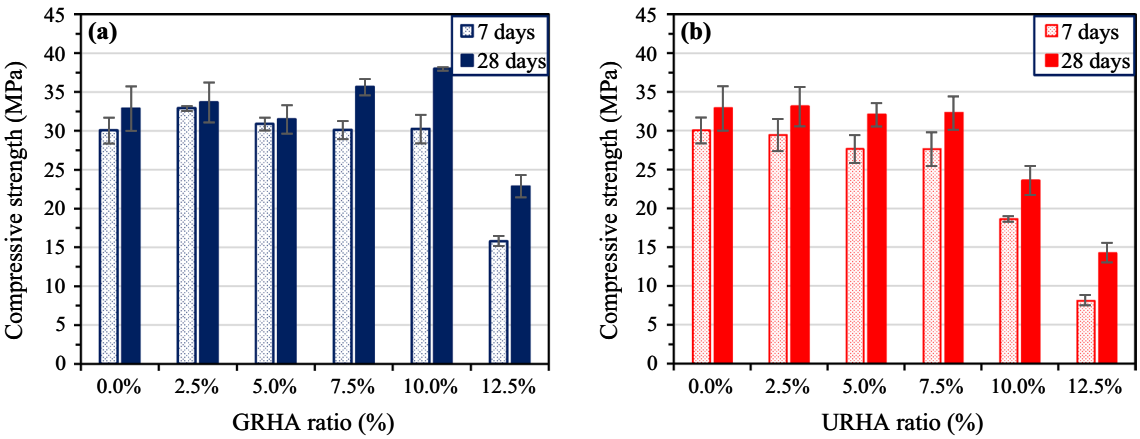

Fig. 10 Compressive strength development of: **a** GRHA-incorporated mixes, and **b** URHA-incorporated mixes

25% from 7 to 28 days of curing age, while this increment ratio varied between 9 and 27% for the mixes containing URHA. As aforementioned, unlike conventional pozzolanic materials, the utilization of fine RHA increases the early age strength (Feng et al. 2004). The test results also verified this as the utilization of GRHA allowed rapid strength gain to yield comparable compressive strength compared to reference at 7 days due to the enhanced pozzolanic reactions. On the other hand, the incorporation of URHA up to 2.5% achieved similar early age strength compared to the reference, and beyond this ratio the 7-day strength reduced.

The compressive strength of mortars containing GRHA was similar or comparable with the REF up to 5% replacement ratio and showed a gradual increment up to 10% replacement at 28 days. The compressive strength of GRHA-10 was obtained as 38.0 MPa at 28 days which is about 16% higher than the REF mixture, indicating optimum utilization ratio. Similar findings were also reported by (Isberto et al. 2019; Krishna et al. 2016), indicating 10% of RHA was optimum for cement-based mortars or concretes. In addition, a significant strength reduction was observed in the GRHA-12.5 sample, possibly resulting from lower compactability and higher porosity as mentioned in Sect. 3.2.2. Furthermore, the higher amount of RHA (> 10%) might have absorbed much more mixing water that is necessary for the hydration of cement and might be another reason for the significant reduction in compressive strength. The inclusion of URHA up to 7.5% resulted in similar compressive strength values compared to the control sample at 28 days, indicating the optimum utilization ratio of URHA. Beyond this ratio, the compressive strength reduced by 27% and 56% compared to the control sample at 28 days in URHA-10 and URHA-12.5 mixes, respectively.

Figure 11 presents the relationship between compressive strength and hardened density of the mixes incorporating RHA and indicates positive and strong relation between the two parameters. It can also be deduced that the relationship between density and compressive strength was statistically insignificant at 7 days, whereas the correlation between these parameters was remarkable at 28 days with R^2 value of 0.95 (Table 3).

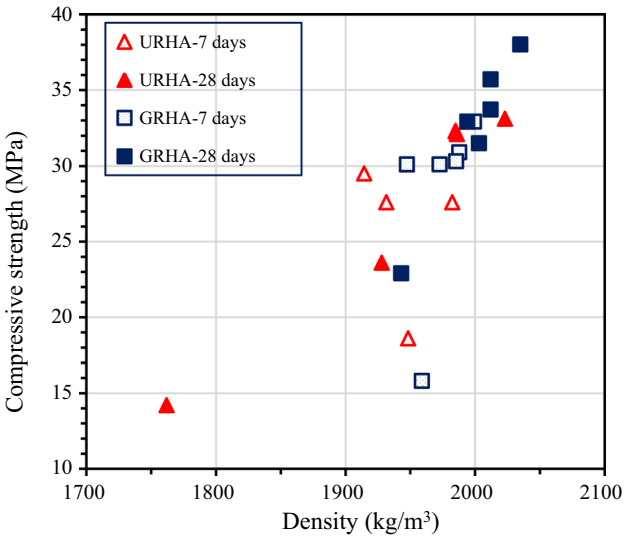

Fig. 11 Relationship between density and compressive strength

3.3 Microstructural Investigation

3.3.1 Thermogravimetric Analysis (TGA)

Figure 12 shows the variation of thermogravimetric curves with the incorporation of GRHA or URHA. The TG/DTG curves revealed the expected responses appearing in cement matrix once exposed to a systematic heating rate from 25 to 1000 °C. It was seen that all the specimens sustained temperatures up to 1000 °C. The total mass loss values varied in a narrow range between 21.3 and 21.8%. The maximum mass loss was observed in mixes containing 10% of URHA, whereas the GRHA-10 had the lowest mass loss than that of others. The DTG curves were derived using the mass loss data and are shown in Fig. 12b, in order to determine the boundaries of the different reaction products. The prominent peaks located at around 120 °C denote the mass loss of physically bound water. The dehydration of silicate gels like C–S–H and the dissociation of ettringite occurred at the temperature range between 120 and 400 °C (Kabay et al. 2021b). The other peaks between approximately 400–480 °C indicate the dehydration of $Ca(OH)_2$ (Snehal et al. 2020a, b; Snehal et al. 2020a, b), and the peaks between 700 and 800 °C show the degradation of $CaCO_3$ (Das et al. 2018; Kabay et al. 2021b). The higher mass loss at around 25–120 °C was observed in 10% URHA-containing mortar, which is mainly due to the evaporation of weakly bounded water, indicating lower reaction product formation compared to the others. This result is in line with the compressive strength results. Moreover, the decomposition level of C–S–H and ettringite was found to be similar for all specimens. For the samples REF, URHA-10, and GRHA-10, the mass losses of samples corresponding to $Ca(OH)_2$ were approximately 2.36%, 2.08%, and 1.59%, respectively. The quantities of $Ca(OH)_2$ of REF, URHA-10, and GRHA-10 were obtained as 9.70%, 8.55%, and 6.53%, respectively. These evident reductions in the portlandite content with the incorporation of GRHA or URHA show that the utilization of GRHA or URHA contributes to the hydration reactions by consuming portlandite due to their pozzolanic reactivities. In addition, the higher reduction of GRHA-incorporated mixes denotes the effect of fineness on the pozzolanic activity; the pozzolanic reactivity with portlandite is significantly related with the amount of surface area ready for the hydration (Singh et al.

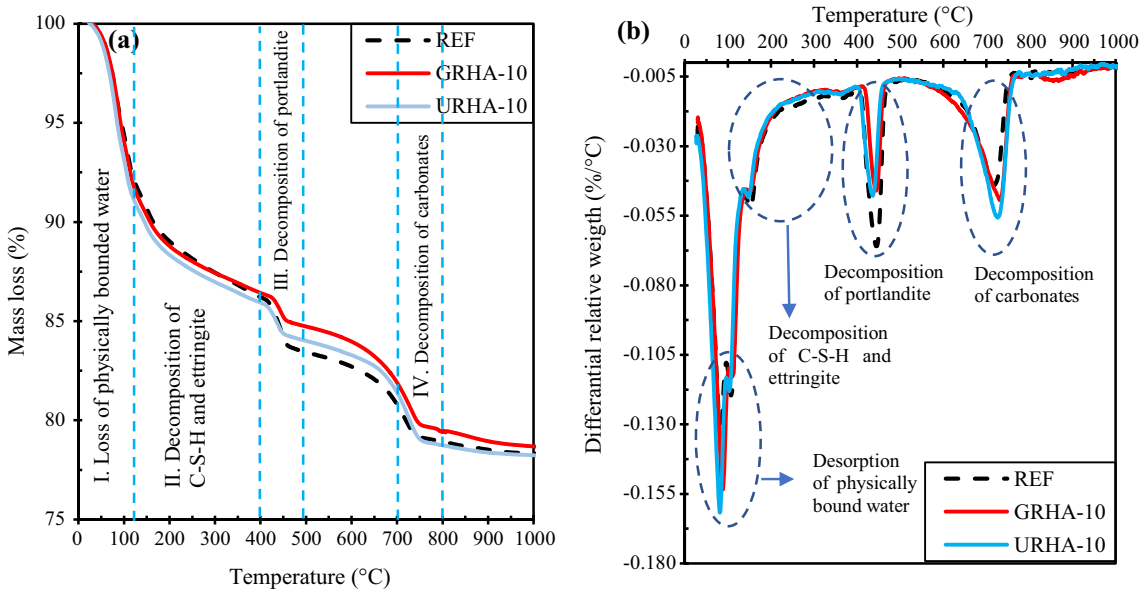

Fig. 12 Thermogravimetric curves of mixes: **a** TG and **b** DTG curves

2015). Hence, the finer RHA particles comparatively allow higher consumption of portlandite. The inclusion of URHA or GRHA evidently increased the intensity of carbonate peaks, and the carbonate peak of URHA-incorporated mixture had the highest intensity. This is possibly due to the higher portlandite consumption of mixes containing RHA, which is then transformed into calcium carbonate (Kabay et al. 2021b; Zeng et al. 2019). In addition, the observed higher carbonate peak in URHA-10 can be attributed to the higher total porosity (see Sect. 3.3.3) which may further induce the carbonation of reaction products such as portlandite and C–S–H (Zeng et al. 2019). It can also be observed from Fig. 13 that the TGA results are compatible with the DTA profiles of mixes which corroborates the evaporation of physically and/or chemically bounded water and the dissociation of portlandite and carbonates (Kabay et al. 2021a; Zhao et al. 2021). Additionally, a significant mass change did not observe for all mixes from 750 to 1000 °C, similar to previously published works (Aly et al. 2012; Petkova et al. 2012).

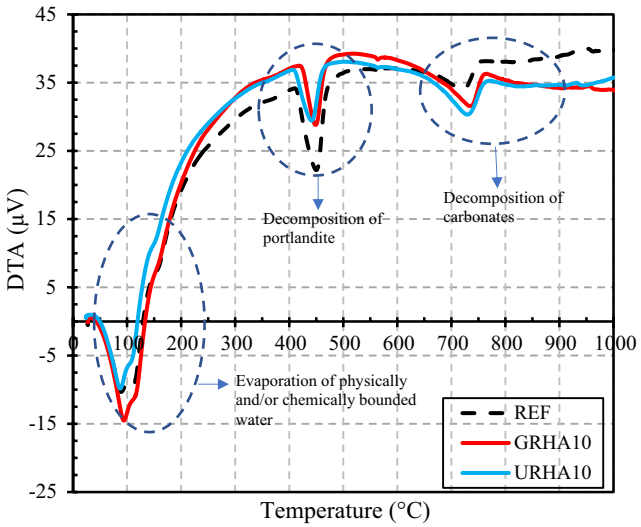

Fig. 13 The DTA curves of mixes

3.3.2 XRD Analysis

The minerological components of paste mixes based on the XRD analysis are illustrated in Fig. 14. The prominent peaks are described as Quartz (#PDF 01-089-1961), Portlandite (#PDF 01-084-1271), Calcite (#PDF 98–002-3975), C–S–H (#PDF 00-033-0306), Ettringite (#PDF 01-072-0646), and the traces of C_3S and C_2S (#PDF 01-087-1260) which comes from clinker for all specimens. The intense quartz (SiO_2) peaks were mainly observed located at around 21° and 26° (2θ), and the portlandite peaks were detected throughout the diffraction patterns for all mixes. On the other hand, the slight disparities were observed in XRD patterns. The peak intensities of portlandite at around 18° and 34° (2θ) reduced with the incorporation of 10% GRHA, indicating its consumption via pozzolanic activity. This result is compatible with the TGA/DTA analysis. In addition, the quartz peaks showed an increment with the addition of GRHA and URHA due to the abundant presence of SiO_2 within the RHA. XRD pattern of URHA-10 exhibited mostly crystalline structure, and the peak intensities of quartz and portlandite increased

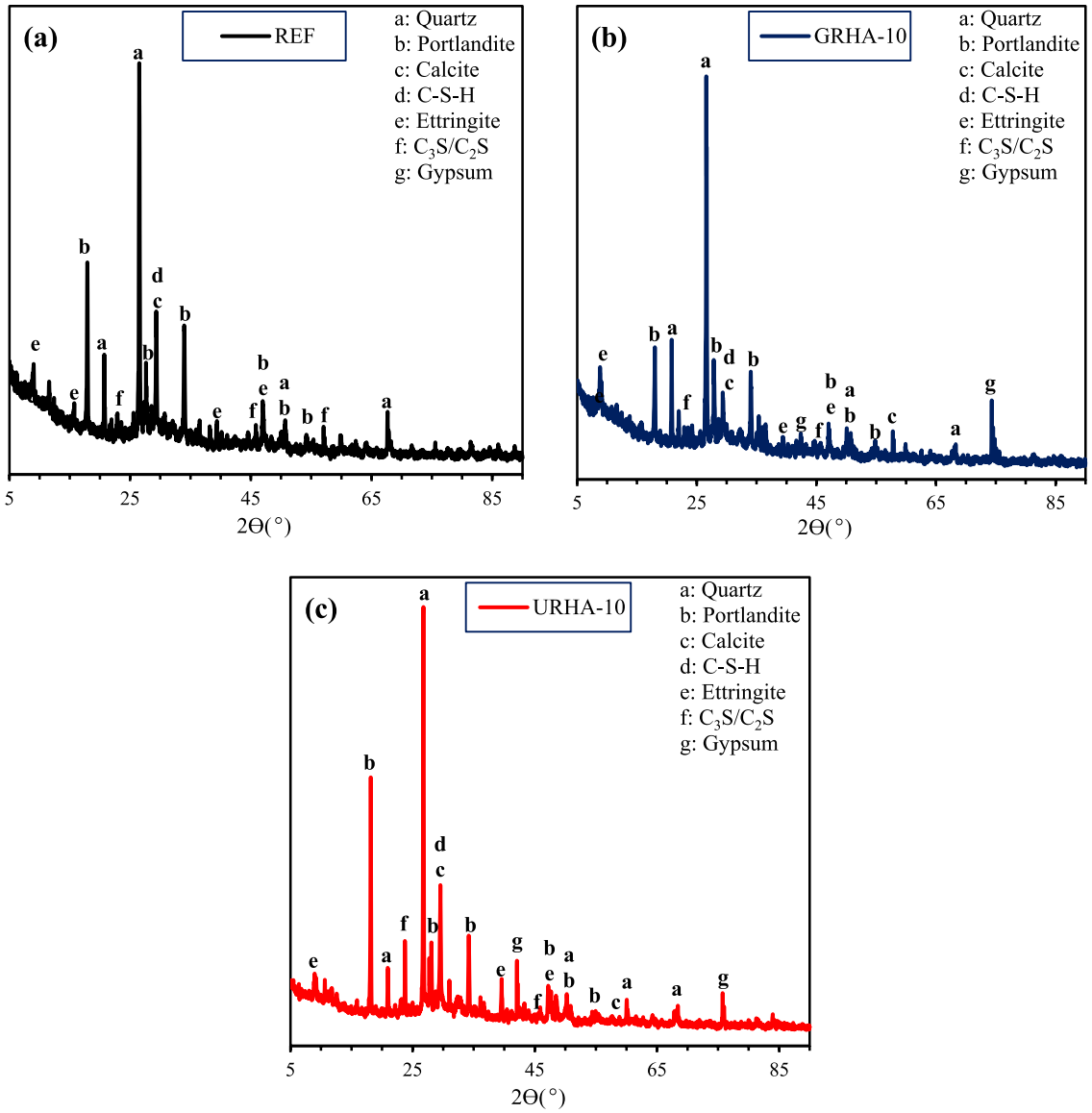

Fig. 14 The diffraction patterns of mixes: **a** REF, **b** GRHA-10, and **c** URHA-10

with the inclusion of 10% URHA, which verifies the lower compressive strength of the URHA-10 specimen. The gypsum peaks (#PDF 01-073-1942) were observed in the XRD pattern of GRHA- and URHA-incorporated mixes different from the REF mixture. The formation of this peak may indicate the lower formation of ettringite in those mixes.

3.3.3 MIP Analysis

The porosimetry analysis based on MIP was performed to investigate the pore structure and the effect of GRHA or URHA on mortar samples. The porosimetry results of mortars at 28 days of curing age are depicted in Figs. 15 and 16. The pore structure was categorized as small capillary pores (< 0.1 μm), large capillary pores (0.1–1.0 μm), and macro-pores (> 1.0 μm) (Song et al. 2019), and the pore parameters, including critical and average pore size along with the total porosity, are listed in Table 4. It can be noticed that the capillary pores constituted the majority of the total porosity, and the capillary pores were found as 75%, 83%, and 82% for the REF, GRHA-10, and URHA-10, respectively. In addition, the small capillary pores occupied the prevalence of the total capillary pores. REF had fewer capillary pores compared to the mortars containing RHA, while URHA-10 comprised the highest proportion of capillary pores. On the contrary, the REF mixture encompassed the highest macro-pores, which is 1.48 and 1.17 times higher than the

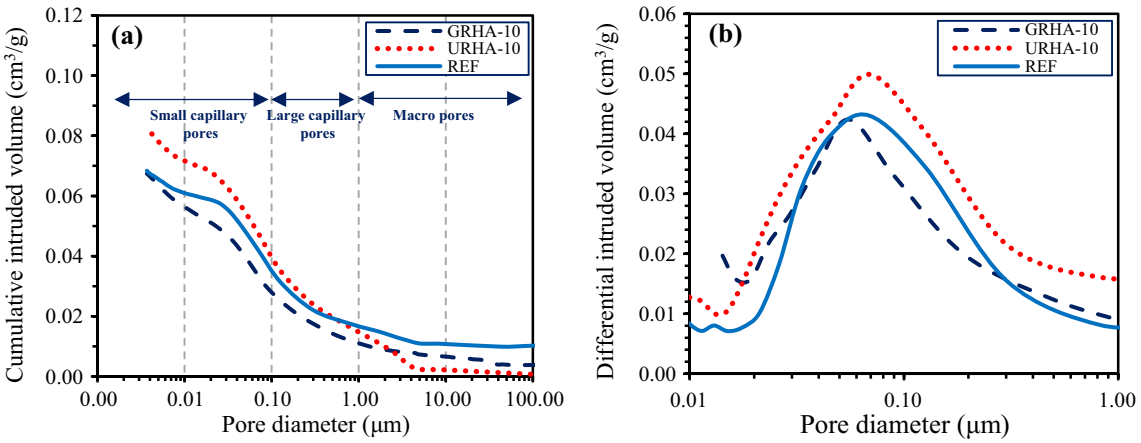

Fig. 15 MIP results of mortar specimens: **a** pore size distribution, and **b** differential curves

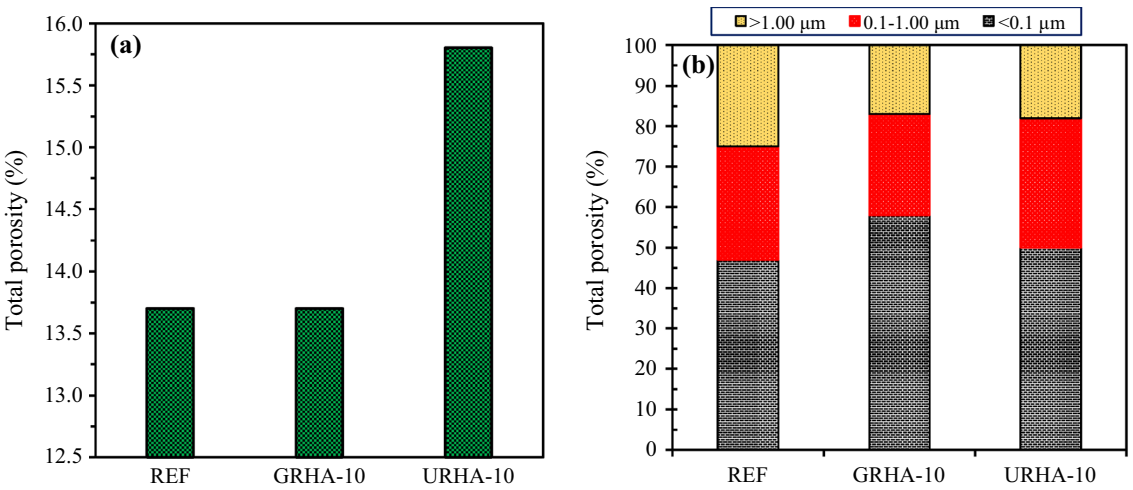

Fig. 16 **a** The total porosity of mortar samples, **b** the distribution of pore size ranges in total porosity

Table 4 The pore parameters of the mortar specimens

Sample code	Critical pore size (μm)	Average pore size (μm)	Capillary pores (%)		Macro-pores (%)	Total porosity (%)
			Small	Large		
REF	0.043	0.008	6.4	3.9	3.4	13.7
GRHA-10	0.042	0.006	7.9	3.5	2.3	13.7
URHA-10	0.050	0.007	7.9	5.0	2.9	15.8

GRHA-10 and URHA-10, respectively. The total porosities were determined as 13.7%, 13.7%, and 15.8% for REF, GRHA-10 and URHA-10, respectively. The critical and average pore size values decreased with the inclusion of 10% GRHA, whereas an increase was observed with the addition 10% URHA. The MIP analysis results are in well agreement with the physico-mechanical test results of the mortars. Among the investigated mortars, the highest compressive strength was found in GRHA-10 which might be attributed to its lowest macro-pore content, and the lowest compressive strength was obtained in the URHA-10 mixture which might be due to the highest total porosity and increased critical pore size.

4 Conclusions

This paper experimentally analyzed the effect of ground and unground RHA on the fresh, physico-mechanical, and microstructural properties of cementitious mortars. Based on the scope of the experimental study, the following bullet points can be drawn:

- The incorporation of GRHA and URHA consistently reduced the fluidity of mortar mixes. The GRHA provided better workability compared to URHA for their corresponding replacement ratios which was due to its more compact structure verified by SEM analysis.
- The porosity of mortar specimens increased with the addition of URHA at 7 and 28 days, while the addition of GRHA efficiently reduced the porosity values compared to the reference. The water absorption of mortar mixes exhibited a similar tendency with porosity values where higher porosity induced higher water absorption, irrespective of the curing age or RHA type used.
- The compressive strength of GRHA- or URHA-incorporated mortars performed similar or comparable compressive strength values up to 7.5% replacement ratio. GRHA-10 mortars exhibited the highest compressive strength of 38 MPa at 28 days, while the inclusion of URHA beyond 7.5% caused significant drops in strength.
- TGA and XRD results indicated that the utilization of both GRHA and URHA significantly reduced the portlandite content. Besides, GRHA addition induced higher portlandite consumption indicating higher pozzolanic reactivity. The MIP test results showed consistent results with the compressive strength.
- In general, the utilization of GRHA up to 10% replacement ratio for producing cement mortar samples can be beneficial in terms of improved physico-mechanical properties compared to the control mortar mixture. On the other hand, even though the physical properties were negatively affected by the inclusion of URHA, the compressive strength value of URHA mix was similar to that of control mixture up to 7.5% replacement ratio which indicates an optimum ratio to utilize in cement-based mortars. Therefore, the utilization of URHA in cement-based mortars up to 7.5% may also be an alternative to GRHA which also reduces the cost of grinding.

Acknowledgements The experimental studies were conducted at Construction Materials Laboratory of Yildiz Technical University. The first author would like to thank Yildiz Technical University Erasmus+ Service for their supports throughout the Erasmus mobility.

Declarations

Conflict of interest The authors declare that they have no potential conflict of interest in this manuscript.

References

Abdulmatin A, Khongpermgoson PS, Sanit-in S, Jaturapitakkul C, Tangchirapat W, Khomwan N, Pham TM (2022) Bottom ash as an alternative pozzolanic material to produce eco-friendly, high-quality chloride-resistant concrete. Iran J Sci Technol Trans Civ Eng. https://doi.org/10.1007/s40996-022-00932-8

Abu Bakar BH, Ramadhansyah PJ, Megat Azmi MJ (2011) Effect of rice husk ash fineness on the chemical and physical properties of concrete. Mag Concr Res 63(5):313–320

Aly M, Hashmi MSJ, Olabi AG, Messeiry M, Abadir EF, Hussain AI (2012) Effect of colloidal nano-silica on the mechanical and physical behaviour of waste-glass cement mortar. Mater Des 33:127–135

Antiohos SK, Papadakis VG, Tsimas S (2014) Rice husk ash (RHA) effectiveness in cement and concrete as a function of reactive silica and fineness. Cem Concr Res 61–62:20–27. https://doi.org/10.1016/j.cemconres.2014.04.001

Bouzón N, Payá J, Borrachero MV, Soriano L, Tashima MM, Monzó J (2014) Refluxed rice husk ash/NaOH suspension for preparing alkali activated binders. Mater Lett 115:72–74

Chithra S, Kumar SRRS, Chinnaraju K (2016) The effect of colloidal nano-silica on workability, mechanical and durability properties of high performance concrete with copper slag as partial fine aggregate. Constr Build Mater 113:794–804

Cordeiro GC, Toledo Filho RD, de Moraes Rego Fairbairn E (2009) Use of ultrafine rice husk ash with high-carbon content as pozzolan in high performance concrete. Mater Struct 42(7):983–992

Costa JAS, Paranhos CM (2018) Systematic evaluation of amorphous silica production from rice husk ashes. J Clean Prod 192:688–697

Das S, Aguayo M, Kabay N, Mobasher B, Sant G, Neithalath N (2018) Elucidating the influences of compliant microscale inclusions on the fracture behavior of cementitious composites. Cement Concr Compos 94:13–23

Feng Q, Yamamichi H, Shoya M, Sugita S (2004) Study on the pozzolanic properties of rice husk ash by hydrochloric acid pretreatment. Cem Concr Res 34(3):521–526

Fernando S, Nasvi MCM, Gunasekara C, Law DW, Setunge S, Dissanayake R (2021) Systematic review on alkali-activated binders blended with rice husk ash. J Mater Civ Eng 33(9):04021229

Ferraro RM, Nanni A, Vempati RK, Matta F (2010) Carbon neutral off-white rice husk ash as a partial white cement replacement. J Mater Civ Eng 22(10):1078–1083

Gil-Carrera L, Browne JD, Kilgallon I, Murphy JD (2019) Feasibility study of an off-grid biomethane mobile solution for agri-waste. Appl Energy 239:471–481

Hadipramana J, Riza FV, Rahman IA, Loon LY, Adnan SH, Zaidi AMA (2016) Pozzolanic characterization of waste Rice husk ash (RHA) from Muar, Malaysia. IOP Conf Ser Mater Sci Eng 160(1):012066

Isberto CD, Labra KL, Landicho JMB, de Jesus R (2019) Optimized preparation of rice husk ash (Rha) as a supplementary cementitious material. GEOMATE J 16(57):56–61

Jamil M, Kaish A, Raman SN, Zain MFM (2013) Pozzolanic contribution of rice husk ash in cementitious system. Constr Build Mater 47:588–593

Jongpradist P, Homtragoon W, Sukkarak R, Kongkitkul W, Jamsawang P (2018) Efficiency of rice husk ash as cementitious material in high-strength cement-admixed clay. Adv Civ Eng 2018:8346319

Kabay N, Miyan N, Özkan H (2021a) Basic oxygen furnace and ground granulated blast furnace slag based alkali-activated pastes: characterization and optimization. J Clean Prod 327:129483

Kabay N, Miyan N, Özkan H (2021b) Utilization of pumice powder and glass microspheres in cement mortar using paste replacement methodology. Constr Build Mater 282:122691

Krishna NK, Sandeep S, Mini KM (2016) Study on concrete with partial replacement of cement by rice husk ash. IOP Conf Ser Mater Sci Eng 149(1):012109

Liu X, Chen X, Yang L, Chen H, Tian Y, Wang Z (2016) A review on recent advances in the comprehensive application of rice husk ash. Res Chem Intermed 42(2):893–913

Malhotra VM, Mehta PK (1996) Pozzolanic and cementitious materials, vol 1. Taylor & Francis, Abingdon

Moayedi H, Aghel B, Nguyen H, Rashid ASA (2019) Applications of rice husk ash as green and sustainable biomass. J Clean Prod 237:117851

Mounika G, Baskar R, Sri Kalyana Rama J (2022) Rice husk ash as a potential supplementary cementitious material in concrete solution towards sustainable construction. Innov Infrastruct Solut 7(1):1–14

Mukharjee BB, Patra RK (2022) Effect of coarse recycled aggregate and rice husk ash on concrete: a factorial design approach. Iran J Sci Technol Trans Civ Eng 46:1–17

Mymrin V, Pedroso DE, Pedroso C, Alekseev K, Avanci MA, Winter E Jr, Cechin L, Rolim PHB, Iarozinski A, Catai RE (2018) Environmentally clean composites with hazardous aluminum anodizing sludge, concrete waste, and lime production waste. J Clean Prod 174:380–388

Nair DG, Fraaij A, Klaassen AAK, Kentgens APM (2008) A structural investigation relating to the pozzolanic activity of rice husk ashes. Cem Concr Res 38(6):861–869

Petkova V, Stoyanov V, Pelovski Y (2012) TG–DTG–DTA in studying white self-compacting cement mortars. J Therm Anal Calorim 109(2):797–806

Sanou I, Sawadogo M, Seynou M, Zerbo L, Ouedraogo R (2019) Study of the mechanical behaviour of mortars modified with rice husk ash. J Miner Mater Charact Eng 7(6):373–384

Sarangi M, Bhattacharyya S, Behera RC (2009) Effect of temperature on morphology and phase transformations of nano-crystalline silica obtained from rice husk. Phase Transitions 82(5):377–386

Siddika A, al Mamun MA, Alyousef R, Mohammadhosseini H (2021) State-of-the-art-review on rice husk ash: a supplementary cementitious material in concrete. J King Saud Univ Eng Sci 33(5):294–307

Singh LP, Goel A, Bhattachharyya SK, Ahalawat S, Sharma U, Mishra G (2015) Effect of morphology and dispersibility of silica nanoparticles on the mechanical behaviour of cement mortar. Int J Concr Struct Mater 9(2):207–217

Snehal K, Das BB, Akanksha M (2020a) Early age, hydration, mechanical and microstructure properties of nano-silica blended cementitious composites. Constr Build Mater 233:117212

Snehal K, Das BB, Kumar S (2020b) Influence of integration of phase change materials on hydration and microstructure properties of nanosilica admixed cementitious mortar. J Mater Civ Eng 32(6):04020108

Snehal K, Das BB, Sudhi A, Pandey D (2022) Pozzolanic reactivity, hydration and microstructure characteristics of blended cementitious composites comprising of ultrafine particles. Iran J Sci Technol Trans Civ Eng 46:1–18

Song Y, Zhou J, Bian Z, Dai G (2019) Pore structure characterization of hardened cement paste by multiple methods. Adv Mater Sci Eng 2019:3726953

Tuoi Nguyen V, Tran TT, Nguyen XT, Tran TM, Quyet Truong V (2022) Effect of natural pozzolanic additive on strength and durability of concrete immersed in seawater. Iran J Sci Technol Trans Civ Eng. https://doi.org/10.1007/s40996-022-00961-3

Zaid O, Ahmad J, Siddique MS, Aslam F (2021) Effect of incorporation of rice husk ash instead of cement on the performance of steel fibers reinforced concrete. Front Mater. https://doi.org/10.3389/fmats.2021.665625

Zain MFM, Islam MN, Mahmud F, Jamil M (2011) Production of rice husk ash for use in concrete as a supplementary cementitious material. Constr Build Mater 25(2):798–805

Zeng Q, Fang R, Li H, Peng Y, Wang J (2019) Tailoring the thermal and mechanical properties of lightweight cement-based composites by macro and micro fillers. Cem Concr Compos 102:169–184

Zerbino R, Giaccio G, Isaia GC (2011) Concrete incorporating rice-husk ash without processing. Constr Build Mater 25(1):371–378

Zhao J, Wang K, Wang S, Wang Z, Yang Z, Shumuye ED, Gong X (2021) Effect of elevated temperature on mechanical properties of high-volume fly ash-based geopolymer concrete, mortar and paste cured at room temperature. Polymers 13(9):1473